IFIT1 is an antiviral protein that recognises 5'-triphosphate RNA

Giulio Superti-Furga, Andreas Pichlmair, Caroline Lassnig, Christoph L Baumann, Tilmann Bürckstümmer, Thomas R Burkard, Adrijana Stefanovic, Keiryn Bennet, Jacques Colinge, Thomas Rülicke, et al.

IFIT1 is an antiviral protein that recognises 5'-triphosphate RNA

Andreas Pichlmair[1], Caroline Lassnig[2, 3], Carol-Ann Eberle[1], Maria W Górna[1], Christoph L Baumann[1], Thomas R Burkard[1], Tilmann Bürckstümmer[1], Adrijana Stefanovic[1], Sigurd Krieger[5], Keiryn L Bennett[1], Thomas Rülicke[3, 4], Friedemann Weber[6], Jacques Colinge[1], Mathias Müller[2, 3] and Giulio Superti-Furga[1*]

[1] CeMM- Research Center for Molecular Medicine of the Austrian Academy of Sciences, Vienna, Austria; [2] Institute of Animal Breeding and Genetics, [3] Biomodels Austria and [4] Institute of Laboratory Animal Science, Vetmeduni Vienna, Austria; [5] Department of Clinical Pathology, Medical University of Vienna, Vienna, Austria; [6] Institute for Virology, Philipps University Marburg, Germany

*** Corresponding author:**

Giulio Superti-Furga
CeMM - Research Center for Molecular Medicine of the Austrian Academy of Sciences
Lazarettgasse 14, AKH BT25.3
1090 Vienna, Austria
Email: gsuperti@cemm.oeaw.ac.at
Telephone: +43 664 4042300

Abstract

Antiviral innate immunity relies on recognition of microbial structures. One such structure is viral RNA that carries a triphosphate group on its 5'terminus (PPP-RNA). In an affinity proteomics approach with PPP-RNA as bait we identified interferon induced protein with tetratricopeptide repeats 1 (IFIT1) to mediate binding of a larger protein complex containing other IFIT family members. IFIT1 bound PPP-RNA with nanomolar affinity and required R187 in a highly charged C-terminal groove of the protein. In the absence of IFIT1 growth and pathogenicity of PPP-RNA viruses were severely increased. In contrast, IFITs were dispensable for clearance of pathogens not generating PPP-RNA. Based on this specificity and the high abundance of IFITs after infection we propose that the IFIT complex antagonises viruses by sequestering specific viral nucleic acids.

Pattern recognition receptors (PRRs) sense molecular signatures associated with microbes[1]. Viral nucleic acid delivered and generated during the viral life cycle can activate PRRs to initiate the innate antiviral defence [2]. Recently, triphosphorylated RNA (PPP-RNA), which is constituent of genomic, antigenomic and certain transcript RNAs associated with some viruses like influenza and vesicular stomatitis virus, was identified as one such component that can be recognised by the innate immune system [3-5]. Binding of PPP-RNA to the PRR Retinoic acid inducible gene-I (RIG-I) mediates activation of a signalling cascade that culminates in the expression of type-I interferon (IFN-α/β) and other cytokines [5, 6]. Most likely through evolutionary pressure exerted by the innate immune system, some viruses evolved sophisticated mechanisms to avoid presentation of PPP-RNA[7, 8]. These viruses are often sensed through atypical nucleic acids components such as long double-stranded RNA (dsRNA), which activates Melanoma differentiated associated gene-5 (Mda5) to initiate expression of IFN-α/β [5, 9]. Beside their interferon-inducing capabilities, viral RNAs are known to trigger additional cellular functions that are unrelated to transcriptional control of cytokine expression [2]. Thus, the cellular machinery not only discriminates between host and invading molecules but often selectively targets the same structures as part of an antiviral program execution. Several interferon-stimulated proteins only reveal their antiviral potential after binding to dsRNA [10]. However, some viruses like influenza and Rift valley fever virus appear to generate only limited amounts of long dsRNA [3, 11], yet they are antagonised by IFN-α/β consistent with the notion that alternative viral nucleic acid structures like PPP-RNA may be key to inhibiting their replication. Moreover, there are many early and strongly IFN-α/β-induced proteins that have unclear molecular function and could in principle participate in the machinery involved in engagement of viral nucleic acid some of which have been revealed through viral or host genetics [12-14]. In particular, little is known about the cellular repertoire of proteins that have the potential to bind the type of PPP-RNA that is generated during viral infection. Here we used an unbiased proteomic-centred survey to identify cellular proteins that engage microbial structures [15] and report the identification and functional characterisation of

58 a class of proteins binding to PPP-RNA.

Results

IFIT1 and IFIT-5 are PPP-RNA binding molecules

We used agarose beads coupled to PPP-RNA (mimicking viral RNA) or the same RNA not containing a triphosphate group (OH-RNA), which is known not to activate the innate immune system [3], to affinity purify potentially interacting proteins from HEK293 cells that were or were not pre-treated with recombinant Interferon β (IFN-β). Pulled-down proteins were identified by mass spectrometry (**Supplementary Fig. 1a**). The proteins predominantly precipitated with PPP-RNA from interferon treated cells were interferon stimulated proteins with tetratricopeptide repeats (IFIT) 1-5 (**Supplementary Fig. 1b**). A double-logarithmic plot of the spectral counts as well as the exponential modified protein abundance index (emPAI) [16] confirmed the specific IFN-β dependent enrichment of IFIT1, IFIT2 and IFIT3 (**Fig. 1a**, **Supplementary Fig. 1c**). IFITs were expressed at low levels at steady-state but highly induced by type-I interferon (IFN-α/β) and virus infection [17]. 16 h after treatment with 1000 U/ml hIFN-β, HeLa cells contained 216 pg/µg IFIT1 roughly corresponding to 2.4 million copies per cell (**Fig. 1b**), while in 293T cells the IFIT1 levels were 126 pg/µg, corresponding to some 1.4 million copies (**Supplementary Fig. 2**), placing IFIT1 amongst the most abundant cellular proteins [18]. The IFIT protein family contains four known human (IFIT1, IFIT2, IFIT3, IFIT5) and three mouse members (Ifit1, Ifit-2, Ifit-3) (**Supplementary Fig. 3**). IFITs consist mainly of tetratricopeptide repeats (TPRs) but no annotated nucleic acid binding domain [17]. We tested the binding of IFITs to RNA by using PPP-RNA-coated beads to precipitate human IFITs from IFIT overexpressing 293T cells or using recombinant protein expressed in bacteria. Overexpressed and recombinant IFIT1 and IFIT5, but little IFIT2 and no IFIT3, associated with PPP-RNA beads (**Fig. 1c**, **d**). The two members of the family that best bound to PPP-RNA, IFIT1 and IFIT5, share the highest sequence homology within the IFIT family (**Supplementary Fig. 3**). We

hypothesised that IFIT2 and IFIT 3 associate with PPP-RNA indirectly and be part of a molecular complex that only assembles after IFN-α/β induction.

IFITs form an interferon-dependent multiprotein complex

To study the putative cellular complex assembling around the IFIT family members we performed affinity purification-mass spectrometry (AP-MS) analysis using IFIT1, IFIT 2 and IFIT 3 as baits. We expressed IFIT1, IFIT 2 and IFIT 3 in doxycycline-inducible HEK-FlpIN cells in the presence or absence of IFN-α/β. Doxycycline treatment of HEK-FlpIN cells elicited expression of IFIT1 protein that was comparable to the endogenous levels measured in cells treated with 50 to 500 U/ml of hIFN-β (**Supplementary Fig. 4a**). Moreover, using a green fluorescent protein (GFP)-expressing isogenic cell line it was possible to ascertain that expression in this system is highly homogenous among the cell population (**Supplementary Fig. 4b**). Protein complexes were purified by tandem affinity purification and analysed by Liquid Chromatography-Mass Spectrometry (LC-MSMS)[19, 20]. IFIT proteins interacted with a limited number of cellular proteins in unstimulated cells (**Supplementary Fig. 5**; IntAct database [21] identifier IM-15277). However, IFN-α/β treatment drastically changed the interaction profile in terms of number of identified proteins and peptide count per protein. In purifications from IFN-α/β stimulated cells, IFIT2 and IFIT3 co-purified with IFIT1 with high enough sequence coverage to suggest a stochiometric interaction among the three proteins (**Table 1**). IFIT5 did not co-precipitate with any other IFIT protein. IFITs do not require IFN-α/β-induced factors to bind to each other since tagged versions of IFIT proteins co-precipitated after overexpression of single proteins (**Supplementary Fig. 6a**). Similarly, recombinant purified IFIT1 and IFIT2, IFIT1 and IFIT3 but not IFIT1 and IFIT5 associated in gel filtration experiments, suggesting a direct interaction at a roughly 1:1 ratio (**Fig. 2a, Supplementary Fig. 6b**), consistent with the results obtained by mass spectrometry on cellular complexes. Compiling the individual interaction profiles into a network analysis revealed several interesting features. First, IFN-α/β induced a dramatic change in the number of nodes (**Fig. 2b**), reflecting the fact that the bait proteins are naturally expressed at high levels

only after IFN-α/β induction when they find partners. Also the topology of the network is affected by IFN-α/β stimulation with the dramatic increase of proteins interacting with all three baits from 1 node to 14 nodes (**Fig. 2b**, red dots). At the same time the high degree of connectivity after IFN-α/β validated the quality of the analysis, as contaminants would interact also in non-induced cells. Importantly, the network also suggested that a few inducible components, in this case mainly the IFIT members, may exert their function by recruiting cellular proteins to assemble IFN-triggered cellular machines (**Fig. 2c**). Interestingly, IFIT1B, a poorly characterised member of the IFIT family interacts with both IFIT1 and IFIT3 making it a possible component of the larger complex or of a subcomplex worth investigating in the future (**Fig. 2c**). Among the group of proteins interacting with more than one IFIT member are hnRNP components, known to bind RNA and regulate transport and translation, small nuclear Ribonucleoprotein particle (SNRP) components, RNA binding proteins involved in RNA processing, as well as polyA-binding proteins. While we cannot exclude that these proteins co-precipitate through binding an RNA species that simultaneously binds to IFITs, this is unlikely as it would have to be via an IFN-α/β-inducible RNA. Overall the protein complex suggests a role of IFIT family members in RNA biology. In future, it may be worth investigating the contribution of several members of the IFIT interactome in the antiviral program. Here we initially focus on IFIT1 being the component mediating association of the IFIT complex to PPP-RNA.

Molecular basis for IFIT1 interaction to PPP-RNA

Interferon-stimulated proteins partially re-distribute upon engagement of the respective viral ligands [22]. We examined the subcellular localisation of murine Ifit1 in IFN-β stimulated NIH3T3 cells after transfection of biotinylated PPP-RNA or OH-RNA. Ifit1 is equally distributed in IFN-β treated cells and re-localises to discrete intracellular foci after stimulation with PPP-RNA in roughly half of all cells examined (**Fig. 3a**). In contrast, only a small fraction of cells showed relocalisation of Ifit1 after transfection of OH-RNA.

To further assess the association of PPP-RNA with IFIT1 we investigated the requirement for triphosphates in RNA precipitations comparing cells expressing c-Myc-tagged IFIT1 to cells expressing GFP-RIG-I as positive control. In both cases PPP-RNA was considerably more efficient than its OH counterpart in purifying the two proteins (**Fig. 3b**). Similarly, PPP-RNA efficiently and specifically purified endogenous IFIT1 from both interferon treated HEK293 cells and mouse embryonic fibroblasts (MEFs) (**Fig. 3c**), suggesting that the PPP-RNA binding property of IFIT1 is common to different cells and species. To further assess the PPP-RNA binding properties of IFIT1 we took advantage of *Escherichia coli* purified proteins in gel mobility assays. IFIT1 but not IFIT3 caused mobility retardation of a PPP-RNA and not a OH-RNA probe (**Fig. 3d**). Antibodies directed against the recombinant IFIT1 caused an increased retardation in mobility confirming that IFIT1 is a major component of the retarded complex. IFIT1 contains no recognised RNA binding domain and to identify a potential interaction mechanism we relied on homology modelling with the closest homologue in the PDB database, O-linked β-N-acetylglucosamine transferase (PDB code 1w3b; **Fig. 3e, Supplementary Fig. 7**) [23]. The model shows a superhelical structure of the several tetratricopeptide repeats with an extended groove winding along the longitudinal axis of the protein (**Fig. 3e, Supplementary Fig. 7**). Large patches of positively charged surfaces (blue) can be seen both in the central part of the groove and in C-terminal part of the protein. We identified individual residues different between IFIT1 and IFIT3, mutated these residues into the IFIT3 identity and tested for PPP-RNA binding. Only R187H showed a significant loss of association (**Fig. 3f, Supplementary Fig. 8a**). In these experiments tagged IFIT3 was co-expressed, allowing the demonstration that without a functional PPP-RNA binding moiety, as in the case of the IFIT1(R187H), IFIT3 will not co-purify with PPP-RNA (**Fig. 3f**). Importantly, IFIT1(R187H) maintained its ability to associate with IFIT3 as shown by co-immunoprecipitation experiments and gel filtration (**Supplementary Fig. 8b, c**) indicating that the R187H mutation is not associated with a major folding problem of the protein. To quantify the binding capabilities of wild-type (wt) IFIT1 compared to the mutant we used PPP-RNA- and OH-RNA-coated ELISA plates and found that only the intact IFIT1 displayed a significant affinity for PPP-RNA and none of the other combinations (**Fig. 3g**). To obtain binding

affinities we then used surface plasmon resonance and measured an estimated binding constant of recombinant IFIT1 for PPP-RNA of 242 nM and a 10-20 fold lower affinity of IFIT1 for OH-RNA (3.14 mM) or IFIT1(R187H) for PPP-RNA (4.36 mM) and OH-RNA (2.64 mM) (**Fig. 3h**). Altogether these experiments demonstrate that IFIT1 has the ability to bind directly and specifically to PPP-RNA. Moreover, the data strongly suggest that TPR motifs, such as the ones present in the IFIT1 protein, have the ability to convey specific interactions with nucleic acids, further expanding their well characterised protein-protein interaction property [24].

Sequestration of PPP-RNA by IFIT proteins

Previous studies suggested that IFIT1 suppresses *in vitro* translation through binding eIF3e [17, 25]. While we were able to confirm an overall negative effect of IFITs in PPP-RNA programmed translation assays using rabbit reticulocyte lysates [17, 25], in our experiments it strongly correlated with the RNA-binding properties of the different IFITs. Since the commonly used templates generated by *in vitro* transcription are not capped and contain a triphosphate group at the 5' end our findings suggest a simple mechanism involving PPP-RNA sequestration for the observed inhibitory effects. Accordingly, IFIT1 and IFIT5, the only two family members capable of binding PPP-RNA directly, most efficiently interfered with the assay (**Fig. 4a**). If sequestration was indeed involved it should be antagonised by excess template. To directly test this hypothesis we increased the amount of template RNA and assayed the ensuing translation efficiency. The inhibitory effect of IFIT1 was inversely proportional to the amount of template RNA used in these assays (**Fig. 4b**) and depended on the presence of triphosphates on the 5' end (**Fig. 4c**). To finally prove that it is PPP-RNA binding that lies at the center of the inhibitory effect we used the IFIT1 mutated in R187 to find that IFIT1(R187H) was indeed less effective (**Fig. 4d**). To further exclude any possible interference with the translational machinery based on protein-protein interaction properties we choose the translational assay obtained from wheat germ extract. IFIT1 had an inhibitory effect comparable to the one observed with rodent-derived extracts (**Fig. 4e**). As evolutionary distance between plants and animals dates more than 1.5 billion years [26] and plants do not appear to encode IFIT orthologs [27] it makes specific,

mechanistically meaningful effects on the translational machinery through a protein-protein interaction extremely unlikely. Altogether, this set of data is compatible with the ability of IFIT1 to sequester PPP-RNA and offers a simple mechanism for the negative effects in translational assays.

To test whether IFIT1 has the ability to engage viral RNA also in infected cells, we precipitated tagged IFIT1 or tagged GFP as control from cells infected with vesicular stomatitis virus (VSV) or influenza A virus (FluAV) and tested the association of viral RNA. IFIT1 but not GFP precipitated viral RNA (**Fig. 4f, g**) suggesting that IFIT1 can also bind and potentially sequester viral RNA in cells.

Antiviral effects of IFIT family members

As IFIT1 participates in a protein complex containing stoichiometric amounts of IFIT2 and IFIT3, to test antiviral activity we addressed all three family members and also where appropriate the IFIT1 ortholog IFIT5. Consistent with the requirement for the formation of a protein complex, overexpression of individual family members did not impair virus growth (**Supplementary Fig. 9** and data not shown). siRNA knockdown of IFIT members in HeLa cells effectively and specifically caused reduction of transcript levels and expression of the cognate protein (**Fig. 5a, b, Supplementary Fig. 10 a-d**) but did not influence induction of IFN-β mRNA (**Supplementary Fig. 10e**). Loss of IFIT family members led to an increase in growth of VSV, VSV-M2 (mutated in the Matrix protein, M51R leading to IFN-β induction) and Rift valley fever virus (RVFV Clone13) to different degrees, with IFIT1 and IFIT2 being most efficient (**Fig. 5c-e, Supplementary Fig. 11a-e**). In contrast, growth of encephalomyocarditis virus (EMCV) was not significantly affected by the siRNA treatments (**Fig. 5f, Supplementary Fig. 11f**), consistent with the notion that EMCV does not generate PPP-RNA during its replication cycle [28]. Similar to other PPP-RNA generating viruses, also the replication of FluAV, as measured by activation of a polymerase-I promoter read-out, increased in the absence of IFIT1, IFIT2 and IFIT3, suggesting that the entire IFIT1 complex is involved in antiviral activities against influenza (**Fig. 5g**). Collectively our data suggest that members of the IFIT family contribute to the antiviral response against several PPP-RNA

producing viruses. The contribution of the different family members may differ depending on the nature of the microbial agent. As the affinity of IFIT1 to PPP-RNA constitutes a central feature of the IFIT1 complex, we directly tested its importance for antiviral activity. For this we expressed siRNA-resistant versions of wt IFIT1 and the PPP-RNA binding mutant IFIT1(R187H) (**Fig. 5h**), respectively, in cells that were treated with siRNA against IFIT1. We used as read-out the FluAV polymerase-I dependent transcriptional assay to observe that the PPP-RNA binding impaired IFIT1(R187H) mutant was considerably less able to constrain viral replication as compared to wt IFIT1 (**Fig. 5i**). Taken together these data clearly show that the requirements for an efficient antiviral activity include the presence of all three family members, IFIT1, IFIT2 and IFIT3, and the PPP-RNA binding capability of IFIT1.

Ifit1 displays antiviral activity *in vivo*

Mice should be a particularly suitable model system to study IFIT activity since mouse Ifit1 is the only family member binding PPP-RNA and knockdown cell lines using shRNA against Ifit1 were impaired in their ability to contain virus growth in the presence of IFN-β (**Supplementary Fig. 11 g-j**). We generated mice with a deletion in the *Ifit1* gene (**Fig. 6a**). *Ifit1* deficiency was confirmed by quantitative PCR (**Fig. 6b**) and immunoblotting of lysates from IFN-β stimulated MEFs (**Fig. 6c**). The absence of mouse Ifit1 was not due to defective signalling downstream of the type-I interferon receptor since the interferon responsive protein DAI [29] was induced upon IFN-β treatment (**Fig. 6c**). Under specific pathogen-free (SPF) conditions, mice lacking *Ifit1* showed no phenotypic abnormalities and were undistinguishable from wt C57BL/6 mice.

IFITs have been proposed to regulate cytokine expression [30, 31]. However, Ifit1 deficiency did not change phosphorylation of the transcription factor IRF3 in response to transfection of innate immune stimuli (**Supplementary Fig. 12a**). Transfecting PPP-RNA, viral RNA derived from VSV particles (vRNA), poly-I:C, interferon stimulatory DNA (ISD) or poly-dA:dT, or activation of the TLR pathway through CpG and LPS did not yield significantly different amounts of type-I IFN- and IL-6 protein in MEFs, *ex*

vivo bone-marrow, bone marrow-derived macrophages and bone marrow-derived dendritic cells (**Fig. 6d, Supplementary Fig. 12b-g**). Neither was the induction of IFN-α/β and IL-6 protein by viral infection affected by *Ifit1*deficiency (data not shown). We therefore concluded that Ifit1 is dispensable for induction of antiviral cytokines. In contrast, Ifit1-deficient cells allowed consistent higher VSV accumulation compared to wt counterparts at three different time points tested (**Fig. 6e**). EMCV infected MEFs showed equal viral loads irrespective of the genetic status of the Ifit1 gene (**Fig. 6f**).

To establish an antiviral function of Ifit1 *in vivo* we infected *Ifit1* knockout mice with VSV. At all doses tested, Ifit1 deficient mice showed significantly reduced survival as compared to control mice (**Fig. 6g, Supplementary Fig. 13a** and data not shown), suggesting that control of VSV infection required Ifit1 also *in vivo*. In contrast, absence of Ifit1 did not affect viability of mice infected with EMCV (**Fig. 6h, Supplementary Fig. 13b**). Similar to EMCV, Ifit1 seemed to be dispensable for the clearance of *Listeria monocytogenes*, a bacterium known to predominantly engage DNA-sensing pathways [32, 33] (**Fig. 6i, Supplementary Fig. 13c**). We concluded that *in vivo*, Ifit1 manifests a critical activity against VSV and presumably other PPP-RNA-expressing viruses but not against the other pathogens tested here.

Overall we conclude that the IFIT proteins contribute to an executing branch of the PPP-RNA innate immunity molecular network. While RIG-I represents the PPP-RNA sensing module that signals towards type-I interferon production, interferon causes a feed-back mechanism that ensures the arming of cells with PPP-RNA-binding antiviral proteins, such as IFIT1, IFIT5 and the protein complexes that they form. (**Supplementary Fig. 14**).

Discussion

IFIT1 demands the regular attention of immunologists, since it is encoded by one of the most abundantly IFN-α/β induced mRNAs. So far most evidence has been gathered for it being a general inhibitor of protein translation [17]. Recently, however, elegant studies using viruses defective in their ability to methylate mRNA CAP structures at the 2'O-position and *Ifit1* and *Ifit2* deficient mice identified an intriguing correlation between specific 5'nucleic acid conformations and Ifit function [14] for which the present study offers a mechanistic rationale. While IFIT1 is shown here to bind PPP-RNA, IFIT2 and IFIT3 also have a virus-containing function and all three proteins form a complex that contains yet other family members as well as other RNA-binding proteins. This raises the possibility that the IFIT complex represents multiple RNA-binding valencies able to recognise and counteract a yet to be determined spectrum of microbes. The IFIT versatility may well reside in the modular use of TPRs, shown here to have nucleic acid binding capability, in analogy to the role of leucine-rich repeats that confer binding plasticity to another family of PRR, namely the Toll-like receptors. Unlike these, IFITs are strongly induced during infection and reach expression levels beyond a million copies per cell. This abundance, rather than with the signalling roles of receptors, may be more compatible with an executing function. We therefore suggest a general model whereby IFIT proteins exert their antiviral activity by physically engaging microbial elements. In particular the present work focuses on the 5'conformation of RNAs such as it is present on the genomic, antigenomic and some transcripts of certain virus species. While members of the RIG-I helicases represent the PPP-RNA binding components of the sensing and interferon induction branch of the innate immunity molecular network, we here propose that IFIT family members represent the PPP-RNA binding component of an executing antiviral branch of the network. The final fate of the PPP-RNA physically sequestered by the IFIT complex remains to be elucidated. Sequestration of viral components has been described before in the case of orthomyxovirus resistance (Mx) proteins known to physically inhibit assembly of viral particles though binding viral proteins [34]. Some viruses

generate large amounts of small triphosphorylated leader-RNAs which could potentially antagonise IFIT activity [35]. We suggest that similarly to the diverse set of proteins sensing the variety of PAMPs and triggering the anti-pathogen response, also the abundant proteins executing the response itself need to maintain specificity for defined pathogen structures to limit interference with vital host processes.

Database accession numbers

Mass spectrometry data presented in Figure 2 was deposited in the IntAct database [21], identifier: IM-15277.

Table 1

	Bait protein					
	IFIT1		**IFIT2**		**IFIT3**	
	No IFN	**+ IFN**	**No IFN**	**+ IFN**	**No IFN**	**+ IFN**
IFIT1	19	34	5	29	14	32
IFIT2	0	17	24	25	0	19
IFIT3	0	29	5	25	32	28
IFIT5	0	0	0	0	0	0

HEK-FlpIN cells were stimulated with 1 μg/ml doxycycline for 24 h to induce expression of IFIT1. Cells were left untreated or treated overnight with approximately 1000 U/ml IFN-α/β that was generated by transfecting HEK293 cells with poly-I:C. Protein complexes isolated by tandem affinity purification were analysed by LC-MSMS. The table shows number of identified IFIT peptides in precipitations of IFITs (Bait proteins) in presence or absence of IFN-α/β, as indicated.

Figure Legends

Figure 1: Identification of an IFN-α/β-induced IFIT containing complex as a PPP-RNA binding entity

(a) HEK293 cells were left untreated or treated with 1000 U/ml IFN-β overnight. Cells were lysed and incubated with PPP-RNA or OH-RNA coupled to streptavidin beads. After precipitation, bead-associated proteins were eluted, separated by 1D SDS PAGE electrophoresis and whole lanes analysed by Liquid Chromatography-Mass Spectrometry (LC-MSMS). Identified proteins are represented as dots with detection strength (log of spectral count) in OH-RNA pull downs (x-axis) and PPP-RNA pull downs (y-axis), both in IFN-β stimulated conditions. Red dots represent proteins with no detection in the absence of IFN-β in both OH-RNA and PPP-RNA pull downs. IFIT proteins are by far the strongest hits. IFIT5 is gray due to detection in the pull down done in the absence of IFN-β priming. Data from four experiments is shown. **(b)** 10^6 HeLa cells were treated with the indicated amount of recombinant IFN-β for 16h and the lysates, alongside a recombinant IFIT1 standard, were analysed by immunoblotting for IFIT1 and tubulin. The signal was quantified using infrared imaging. The cellular copy number of IFIT1 in per HeLa cells treated with 1000 U/ml IFN-β was determined to be $2{,}4 * 10^6$. One of two experiments done in duplicate is shown. **(c, d)** Lysates from 293T cells transfected with plasmids for c-Myc-tagged IFITs **(c)** and *E. coli* expressing His-GST-tagged IFITs **(d)** were used for affinity precipitation with PPP-RNA and associated proteins analysed by immunoblotting.

Figure 2: Formation of a complex containing IFIT proteins

(a) Recombinant IFIT proteins and their binary complexes were analyzed by size-exclusion chromatography. Shown are overlaid elution profiles from Superdex 200 10/300 GL column (the void volume is ~8.3 ml), and the indicated peak fractions were analyzed by SDS-PAGE followed by coomassie staining. His-tagged IFIT1 binds His-GST-tagged IFIT2. **(b, c)** Network analysis of the IFIT protein complex based on data described in Table 1. **(b)** The IFIT proteins (large balls) in absence of IFN-α/β stimulation (left) are interacting with fewer proteins (small balls) whereas upon IFN-α/β stimulation IFITs recruit many new partners. Interactions between IFIT-1, -2, and -3 are also stronger. Proteins identified by all IFITs are shown in red. **(c)** Protein interaction network for the IFN-α/β stimulated condition and annotated protein functions using Gene Ontology (GO) molecular functions and manual curation. Obvious non-specific proteins or contaminants were removed (keratin, albumin from MS BSA quality control runs, and MCC12 and PCCAB which bind to the Strep-tactin affinity resin in high abundance). Many of the shared IFIT partners have the ability to bind to RNA (red) and some are involved in mRNA translation (green). IFIT bait proteins are shown in blue.

Figure 3: Triphosphate-dependent RNA-binding of IFIT1 requires an Arginine at position 187

(a) Ifit1 redistribution (white arrows) in IFN-β - treated NIH 3T3 cells transfected with biotinylated PPP-RNA and OH-RNA for 3 h. Shown is the average % relocalisation of Ifit1 (+/- standard deviation) in 100 randomly selected cells in two independent experiments. * = $p < 0,05$. **(b, c)** PPP-RNA or OH-RNA beads were used for affinity purification from lysates of 293T cells expressing c-Myc-IFIT1 or GFP-RIG-I **(b)** or IFN-β treated HEK293 cells and MEFs **(c).** Precipitates were analysed by immunoblotting. **(d)** Mobility shift assay of PPP-RNA and OH-RNA by recombinant His- GST-IFIT1 and -IFIT3. Where indicated an antibody against GST was added. Numbers on the right indicate free probe (1), shifted probe (2) and supershifted probe (3). **(e)** Surface charge of an IFIT1 structure model based on O-linked β-N-acetylglucosamine transferase (PDB code 1w3b). Surface colour represents electrostatic potential, red is

negative, blue is positive charge, N is N-terminus, C is C-terminus. Proteins with targeted point mutations of the indicated residues were used for further functional characterisation. **(f)** c-Myc-tagged IFIT1 mutants and HA-IFIT3 were co-expressed in 293T cells and 24 h later used for affinity purification using PPP-RNA as bait. **(g)** PPP-RNA or OH-RNA were bound to ELISA plates and incubated with the indicated amounts (ng) of recombinant IFIT1 or IFIT1(R187H). RNA-asssociated proteins were detected using secondary reagents. Shown is substrate conversion at OD 450, error bars show standard deviation of triplicate measurements. One representative experiment of three is shown. **(h)** The affinity of IFIT1 and IFIT1(R187H) to PPP-RNA and OH-RNA was measured by surface plasmon resonance using biotinylated RNA as immobilised ligand and increasing amounts of recombinant protein. Shown are the response units of the indicated combinations of binding partners with standard deviation from duplicate measurements.

Figure 4: IFIT1 sequesters PPP-RNA *in vitro*

(**a-d**) Rabbit reticulate lysate (RRL) or **(e)** wheat germ extract (WGE) was supplemented with RNA template expressing firefly-luciferase and recombinant IFITs or no protein was added. **(a, d, e)** 0.2 µg of *in vitro* transcribed PPP-RNA template (that is commonly used in such assays) was incubated with the indicated amounts of recombinant IFITs or no protein. **(b)** As in **(a)** but 0.2 µg and 0.05 µg template RNA were used. **(c)** RNA that was not (PPP-luc) or was treated with calf intestinal phosphatase (OH-luc) was supplemented together with 35 µM IFIT1, as indicated. **(d)** Translation of PPP-luc mRNA template in the presence of 35 µM IFIT3, IFIT1 or IFIT1(R187H). **(a-e)** The graph shows luciferase activity after an 1 h incubation period at 37 °C. Error bars show standard deviation of at least two experiments done in triplicate measurements. * = $p<0,05$, n.s. = non significant. **(f-g)** HEK-FlpIN IFIT1 or HEK-FlpIN GFP cells were stimulated with doxycycline for 24 h and infected with VSV-GFP and FluAV (both MOI: 5) for 9 h. Cells were then lysed and proteins precipitated using Strep-tactin beads. RNA before (Input) and

after precipitation (SII-IP) was analysed by qRT-PCR for VSV **(f)** or FluAV sequences **(g)**. The graph shows arbitrary units +/- standard deviation of duplicate measurements of one representative experiment of three (f) or two (g).

Figure 5: Influence of IFIT RNA interference on virus growth

(a) 10^5 HeLa cells were transfected with 0.5 µg of the indicated IFIT expression vector and 5 nM siRNA directed against the indicated IFIT family member. Expression of c-Myc-tagged proteins was evaluated by immunoblot 48 h later. **(b-f)** HeLa cells were transfected with 5 nM siRNA for 48 h. **(b)** Cells were stimulated with 0.25 µg PPP-RNA for 16 h and expression of IFIT1 or IFIT3 was tested by immunoblotting. **(c-f)** siRNA treated HeLa cells were infected at a multiplicity of infection (MOI) of 0.01 with VSV **(c)**, VSV-M2 (with a M51R mutation in the matrix protein) [36] **(d)**, RVFV (Clone13) **(e)** or EMCV **(f)** and virus accumulation was tested by TCID50 at 48 h **(c, d, f)** and 72 h **(e)** after infection. Graphs in **(c-f)** show the average of three independent experiments, error bars indicate standard deviation. **(g)** HeLa cells were co-transfected with Pol-I ff-luc (0.1 µg), pRL-TK (0.05 µg) reporter plasmids and the indicated siRNAs. 48 h later cells were left uninfected or infected with FluAV at a MOI of 1 and reporter activity analysed after over-night incubation. The graph shows the ratio between firefly- and renilla luciferase +/- standard deviation of one representative experiment of two done in duplicate measurements. **(h)** HeLa cells were co-transfected with siRNA against IFIT1 or control siRNA together with plasmids coding for c-Myc-tagged versions of parental or silencing-resistant IFIT1. Immunoblots 48 h after transfection are shown. **(i)** as in **(g)** but plasmids coding for silencing-resistant IFIT1 were co-transfected as indicated. The graph shows the ratio between firefly- and renilla luciferase +/- standard deviation of one representative experiment of three done in duplicate measurements.

Figure 6: Ifit1 is necessary to contain virus growth and *in vivo* pathogenicity

(a) Targeting strategy for mouse *Ifit1*. **(b, c)** Loss of Ifit1 in *Ifit1*$^{+/+}$ MEFs (+/+) and *Ifit1*$^{-/-}$ MEFs (-/-) was validated by PCR **(b)** and by immunoblotting in MEFs that were stimulated with IFN-β for 16 h **(c)**. **(d)** MEFs (2 * 10^5 cells/ml) were left unstimulated or transfected with PPP-RNA (0.4 µg/ml and 0.08 µg/ml), viral RNA isolated from VSV particles (vRNA) (0.2 µg/ml), poly-I:C (1 µg/ml) or poly-dA:dT (1 µg/ml) and accumulation of IFN-α/β was tested using a cell line stably containing an ISRE-luc reporter. **(e, f)** MEFs of the indicated genotype were infected with VSV **(e)** or EMCV **(f)** at a MOI of 0.01 and virus accumulation in the cell supernatant was measured by TCID50 after 48 h. Graphs show average virus titers from two independent experiments. Error bars show standard deviation. * = $p<0.05$ tested by two way Annova for two independent experiments done in hexaplicate measurements. **(g-i)** Survival of Ifit1 deficient (*Ifit1*$^{-/-}$) (red lines) and C57BL/6 mice (Ifit*1*$^{+/+}$) (black lines). **(g)** Male animals (n = 14) were anesthetized with ketamine-xylazine and infected intranasally with 10^5 pfu of VSV and monitored twice daily for survival over a two week period. Wt mice survived significantly longer than Ifit deficient animals (Mantel-Cox Test $p < 0.01$). **(h)** Sex-matched *Ifit1*$^{-/-}$ and *Ifit1*$^{+/+}$ mice (n = 17) were infected intraperitoneally with 500 pfu of EMCV and monitored for survival. **(i)** Female *Ifit1*$^{-/-}$ and *Ifit1*$^{+/+}$ mice (n = 9) were infected intraperitoneally with 10^6 CFU *L. monocytognes*. d.p.i.: days post infection.

Acknowledgements

We want to thank the NIH Knock-out Mouse Project (KOMP) for providing ES cells with a targeted Ifit1 allele. We want to thank Lill Andersen for expansion of ES cells, Kumaran Kandasamy for bioinformatics support, Michael Bergmann for providing FluAV matrix protein antibody. The work in the authors' laboratories was funded by the Austrian Academy of Sciences, the i-FIVE ERC grant to GSF, an EMBO long-term fellowship to AP (ATLF 463-2008), a Marie-Curie and an EMBO fellowship to CB, DFG grant We 2616/5-2 and SFB 593/B13 to FW. TR and MM are funded by the Austrian Federal Ministry for Science and Research GEN-AU programme Austromouse; MM is funded by the Austrian Science Fund FWF SFB F28.

Methods

Reagents, proteins and viruses

IFN-α and IFN-β were from PBL Interferonsource. IFN-α/β was generated by transfecting HEK293 cells with poly-I:C. Expression constructs were generated by PCR amplification and cloned into pCS2-6myc-GW, pCDNA-HA-GW, pTO-SII-HA-GW [20] or pETG30A-GW and pETG10A-GW. Point mutations were introduced by site directed mutagenesis. Pol-I ff-luc was from Georg Kochs [37]. p7SK-as and pGFP-RIG-I were described earlier [3]. pRL-TK was from Promega. *In vitro* translation was done with Rabbit reticulocyte lysate or Wheat germ extract (Promega) using the provided luciferase mRNA or SP6-polymerase transcribed luciferase mRNA as template. Strep-tacin beads were from IBA, HA-agarose from Sigma, Protein G sepharose was from GE Healthcare and Streptavidin beads from Pierce. Antibodies for α-tubulin and β-actin were from Alexis. Phospho-IRF3 was from Cell Signalling. IRDye -conjugated anti-myc antibody, anti-mouse and anti-rabbit secondary reagents were from Rockland. Streptavidin Alexa-800, Streptavidin Alexa-488 and goat anti-mouse Alexa-548 were from Molecular probes. Polyclonal antibodies against rb-α–DAI, rb-α–IFIT1, ms-α–Ifit1 and rb-α–IFIT3 were generated by immunisation of animals with full-length recombinant protein. RT-PCR reagents were from Qiagen. Biotinylated PPP-RNA (7SK-as) was described earlier [3]. PPP-RNA was dephosphorylated using Calf intestinal phosphatase (New England biolabs). LPS (E.coli K12), CpG (CpG-DNA-ODN1826), poly-(I:C) and poly-(dA:dT) were from Invitrogen. ISD [33] was synthesised at Microsynth. vRNA was isolated using Trizol (Invitrogen). For stimulation TLR agonists were added other stimuli were transfected with Lipofectamine 2000 (Invitrogen) or Polyfect (Qiagen). Total IFN-α/β was measured as described [38]. IL-6 was measured by ELISA (BD).

Recombinant IFITs were expressed in *E. Coli* and purified on a HisTrap HP column (GE Healthcare). EMCV, FluAV (A/PR/8/34), VSV (strain: Indiana) [38], VSV-GFP [39], VSV-M2 (M51R, originally named

AV1) [36], RVFV (Clone 13) [40] and Listeria monocytogenes (EGD) [41] were described earlier. Viruses were titrated on Vero cells using the TCID50 method of Reed and Muench.

Cells, mice and *in vivo* experiments

293T, NIH3T3 and HEK293 cells were described earlier [3]. IRF3 deficient MEFs were a gift of Thomas Decker. Doxycycline regulatable HEK-FlpIN cells were from Invitrogen. MEFs were generated from embryos of mated Ifit1+/- mice. BM macrophages (BMMs) were cultured in the presence of M-CSF (Prepotech), BM dendritic cells (BM-DC) in presence of GM-CSF (Prepotech). Fibroblasts were kept in DMEM (PAA) and primary cells cultured in RPMI (PAA) supplemented with 10 % fetal calf serum (Invitrogen) and antibiotics (100 U/ml penicillin, 100 µg/ml streptomycin). For inducible transgene expression HEK-FlpIN cells were treated with 1 µg/ml doxycycline for 24-48 h. For siRNA knockdown, 5nmol siRNA was mixed with HiPerfect (Qiagen) and added to 10^5 HeLa cells. 48 h later cells were used for experiments. Sequences of shRNA vectors and siRNA knockdown oligos are available on request. *Ifit1* knockout mice were generated using ES cells clones (VGB6; C57BL/6NTac background) with a targeted *Ifit1* locus. ES cells were provided by the NIH-knockout mouse project (KOMP, NIH). C57BL/6 wild-type control mice were purchased from Charles River. All mice were kept under specific pathogen free conditions according to FELASA recommendations. For EMCV infections age (9-11 weeks) and sex-matched mice were infected intraperitoneally, for Listeria monocytogenes (EGD) age-matched (8-11 weeks) females were infected intraperitonally. For VSV challenge, age-matched (8-11 weeks) male mice were anesthetised with ketamine-xylazine and inoculated intranasally with VSV. All animal experiments were approved by the institutional ethics committee and the Austrian laws (GZ 68.205/0057-II/10b/2010).

RT-PCR, Immunofluorescence, gel shift assays, protein quantification

RNA was isolated using RNeasy kit (Qiagen) and reverse transcribed using oligo-dT primers and the RevertAID RT-PCR kit (Fermentas). NIH3T3 cells were grown overnight on coverslips and stimulated as described in figure legends. Cells were stained with murine anti-Ifit1 antibodies, followed by anti-mouse

Alexa-548, Alexa-488-Streptavidin and DAPI. Images were acquired with a Leica AF6000 deconvolution microscope. For gel shift assays 200 ng biotinylated 7SK-as RNA [3] supplemented with Alexa-800-Streptavidin was incubated with 12,5 µg recombinant His-GST-IFIT1 or His-GST-IFIT3 protein solved in PBS supplemented with RNAsin (Promega) (1:20), DTT (final volume 400 mM) and 100 mM NaCl. Where shown, GST antibody (1 µg) was added. Samples were run on a 1 % Agarose gel and RNA was visualised using a LI-COR Odyssee system. To estimate the protein copy number of IFIT1 in cells, recombinant IFIT1 was used as calibration standard and compared to lysates of IFN-β stimulated HeLa and 293T cells. The signal intensity on western blots was quantified using a LI-COR Odyssee system.

Affinity purifications and measurements, mass spectrometry and homology modelling

For RNA precipitation 5 µg PPP-RNA or OH-RNA (both 7SK-as) were added to streptavidin resin, and incubated with 6 mg of HEK293 cell lysate for 60 minutes. Beads were washed three times in TAP-buffer (50 mM Tris pH 7.5, 100 mM NaCl, 5 % (v/v) glycerol, 0.2 % (v/v) Nonidet-P40, 1.5 mM $MgCl_2$ and protease inhibitor cocktail (Complete, Roche)), proteins eluted by boiling in SDS sample buffer and analysed by one-dimensional SDS-PAGE. Entire gel lanes were anaylsed by mass spectrometry using a hybrid LTQ-Orbitrap XL (ThermoFisher Scientific) or a quadrupole time-of-flight mass spectrometer (QTOF Premier; Waters) coupled to an 1100/1200 series HPLC (Agilent Technologies) with an analytical column packed with C18 material. Data generated by LC-MSMS was searched against UniProtKB/SwissProt version 57.12 [42] integrating Mascot [43] and Phenyx [44] search engines. A false discovery rate of less than 1 % on the protein groups was estimated. HEK-FlpIN cells and isolation of protein complexes for LC-MSMS analysis is described elsewhere [20]. 293T cells were transfected with respective expression plasmids for 48 h and lysates used for immunoprecipitation using HA-agarose or RNA-coated beads. For surface plasmon resonance measurements biotinylated 7SK-as RNA was loaded on a streptavidin coated SA sensor chip (GE Healthcare) and probed with recombinant wild-type or IFIT1(R187H) diluted in running buffer (0.01 M Hepes, pH 7.4, 0.25 M NaCl, 0.005 % surfactant P20). Sensorgrams were fitted to a single site binding model (1:1 Langmuir binding), using the numerical

integration functions of the BIAevaluation 3.1 software package. To determine the dissociation constant (KD) the equilibrium-state binding values were plotted as a function of the applied protein concentrations and fitted to first-order kinetics assuming a monovalent RNA-protein interaction. Comparative modelling was done using the I-TASSER server (http://zhanglab.ccmb.med.umich.edu/I-TASSER/) [45] to obtain a model for full-length IFIT1. The model was based on the structure of O-linked β-N-acetylglucosamine transferase (PDB code 1w3b), with 17 % sequence identity. Surface charge potential was calculated by APBS as implemented in PyMOL (DeLano Scientific).

References

1. Akira, S., Uematsu, S. & Takeuchi, O. Pathogen recognition and innate immunity. *Cell* **124**, 783-801 (2006).
2. Pichlmair, A. & Reis e Sousa, C. Innate recognition of viruses. *Immunity* **27**, 370-383 (2007).
3. Pichlmair, A. *et al.* RIG-I-mediated antiviral responses to single-stranded RNA bearing 5'-phosphates. *Science* **314**, 997-1001 (2006).
4. Hornung, V. *et al.* 5'-Triphosphate RNA is the ligand for RIG-I. *Science* **314**, 994-997 (2006).
5. Yoneyama, M. & Fujita, T. RNA recognition and signal transduction by RIG-I-like receptors. *Immunol Rev* **227**, 54-65 (2009).
6. Schlee, M. *et al.* Approaching the RNA ligand for RIG-I? *Immunol Rev* **227**, 66-74 (2009).
7. Bowie, A.G. & Unterholzner, L. Viral evasion and subversion of pattern-recognition receptor signalling. *Nature reviews* **8**, 911-922 (2008).
8. Schmolke, M. & Garcia-Sastre, A. Evasion of innate and adaptive immune responses by influenza A virus. *Cell Microbiol* **12**, 873-880 (2010).
9. Kato, H. *et al.* Length-dependent recognition of double-stranded ribonucleic acids by retinoic acid-inducible gene-I and melanoma differentiation-associated gene 5. *J Exp Med* **205**, 1601-1610 (2008).
10. Sadler, A.J. & Williams, B.R. Interferon-inducible antiviral effectors. *Nat Rev Immunol* **8**, 559-568 (2008).
11. Weber, F., Wagner, V., Rasmussen, S.B., Hartmann, R. & Paludan, S.R. Double-stranded RNA is produced by positive-strand RNA viruses and DNA viruses but not in detectable amounts by negative-strand RNA viruses. *J Virol* **80**, 5059-5064 (2006).
12. Gay, N.J., Gangloff, M. & O'Neill, L.A. What the Myddosome structure tells us about the initiation of innate immunity. *Trends in immunology* (2011).
13. Ronald, P.C. & Beutler, B. Plant and animal sensors of conserved microbial signatures. *Science* **330**, 1061-1064 (2010).
14. Daffis, S. *et al.* 2'-O methylation of the viral mRNA cap evades host restriction by IFIT family members. *Nature* **468**, 452-456 (2010).
15. Burckstummer, T. *et al.* An orthogonal proteomic-genomic screen identifies AIM2 as a cytoplasmic DNA sensor for the inflammasome. *Nat Immunol* **10**, 266-272 (2009).
16. Ishihama, Y. *et al.* Exponentially modified protein abundance index (emPAI) for estimation of absolute protein amount in proteomics by the number of sequenced peptides per protein. *Mol Cell Proteomics* **4**, 1265-1272 (2005).
17. Guo, J., Hui, D.J., Merrick, W.C. & Sen, G.C. A new pathway of translational regulation mediated by eukaryotic initiation factor 3. *Embo J* **19**, 6891-6899 (2000).
18. Papin, J.A., Hunter, T., Palsson, B.O. & Subramaniam, S. Reconstruction of cellular signalling networks and analysis of their properties. *Nat Rev Mol Cell Biol* **6**, 99-111 (2005).
19. Kocher, T. & Superti-Furga, G. Mass spectrometry-based functional proteomics: from molecular machines to protein networks. *Nature methods* **4**, 807-815 (2007).
20. Glatter, T., Wepf, A., Aebersold, R. & Gstaiger, M. An integrated workflow for charting the human interaction proteome: insights into the PP2A system. *Mol Syst Biol* **5**, 237 (2009).

21. Aranda, B. *et al.* The IntAct molecular interaction database in 2010. *Nucleic acids research* **38**, D525-531 (2010).
22. Reichelt, M., Stertz, S., Krijnse-Locker, J., Haller, O. & Kochs, G. Missorting of LaCrosse virus nucleocapsid protein by the interferon-induced MxA GTPase involves smooth ER membranes. *Traffic* **5**, 772-784 (2004).
23. Jinek, M. *et al.* The superhelical TPR-repeat domain of O-linked GlcNAc transferase exhibits structural similarities to importin alpha. *Nat Struct Mol Biol* **11**, 1001-1007 (2004).
24. D'Andrea, L.D. & Regan, L. TPR proteins: the versatile helix. *Trends in biochemical sciences* **28**, 655-662 (2003).
25. Fensterl, V., White, C.L., Yamashita, M. & Sen, G.C. Novel characteristics of the function and induction of murine p56 family proteins. *J Virol* **82**, 11045-11053 (2008).
26. Wang, D.Y., Kumar, S. & Hedges, S.B. Divergence time estimates for the early history of animal phyla and the origin of plants, animals and fungi. *Proc Biol Sci* **266**, 163-171 (1999).
27. Fensterl, V. & Sen, G.C. The ISG56/IFIT1 gene family. *J Interferon Cytokine Res* **31**, 71-78.
28. Racaniello, V.R. Picornaviridae: The Viruses and Their Replication. *In Fields Virology, D. Knipe, P.M. Howley, D.E. Griffin, R.A. Lamb, M.A. Martin, B. Roizman, and S.E. Straus, eds (Philadelphia: Lippincott Williams & Wilkins)* pp. 685-722 (2001).
29. Takaoka, A. *et al.* DAI (DLM-1/ZBP1) is a cytosolic DNA sensor and an activator of innate immune response. *Nature* **448**, 501-505 (2007).
30. Berchtold, S. *et al.* Forced IFIT-2 expression represses LPS induced TNF-alpha expression at posttranscriptional levels. *BMC Immunol* **9**, 75 (2008).
31. Li, Y. *et al.* ISG56 is a negative-feedback regulator of virus-triggered signaling and cellular antiviral response. *Proc Natl Acad Sci U S A* **106**, 7945-7950 (2009).
32. Sauer, J.D. *et al.* Listeria monocytogenes triggers AIM2-mediated pyroptosis upon infrequent bacteriolysis in the macrophage cytosol. *Cell Host Microbe* **7**, 412-419 (2010).
33. Stetson, D.B. & Medzhitov, R. Recognition of cytosolic DNA activates an IRF3-dependent innate immune response. *Immunity* **24**, 93-103 (2006).
34. Kochs, G., Janzen, C., Hohenberg, H. & Haller, O. Antivirally active MxA protein sequesters La Crosse virus nucleocapsid protein into perinuclear complexes. *Proc Natl Acad Sci U S A* **99**, 3153-3158 (2002).
35. Umbach, J.L., Yen, H.L., Poon, L.L. & Cullen, B.R. Influenza A Virus Expresses High Levels of an Unusual Class of Small Viral Leader RNAs in Infected Cells. *MBio* **1** (2010).
36. Stojdl, D.F. *et al.* VSV strains with defects in their ability to shutdown innate immunity are potent systemic anti-cancer agents. *Cancer Cell* **4**, 263-275 (2003).
37. Dittmann, J. *et al.* Influenza A virus strains differ in sensitivity to the antiviral action of Mx-GTPase. *J Virol* **82**, 3624-3631 (2008).
38. Pichlmair, A. *et al.* Activation of MDA5 requires higher-order RNA structures generated during virus infection. *J Virol* **83**, 10761-10769 (2009).
39. Boritz, E., Gerlach, J., Johnson, J.E. & Rose, J.K. Replication-competent rhabdoviruses with human immunodeficiency virus type 1 coats and green fluorescent protein: entry by a pH-independent pathway. *J Virol* **73**, 6937-6945 (1999).
40. Habjan, M. *et al.* NSs protein of rift valley fever virus induces the specific degradation of the double-stranded RNA-dependent protein kinase. *J Virol* **83**, 4365-4375 (2009).
41. Reutterer, B. *et al.* Type I IFN are host modulators of strain-specific Listeria monocytogenes virulence. *Cell Microbiol* **10**, 1116-1129 (2008).
42. Wu, C.H. *et al.* The Universal Protein Resource (UniProt): an expanding universe of protein information. *Nucleic acids research* **34**, D187-191 (2006).

577 43. Perkins, D.N., Pappin, D.J., Creasy, D.M. & Cottrell, J.S. Probability-based protein identification
578 by searching sequence databases using mass spectrometry data. *Electrophoresis* **20**, 3551-3567
579 (1999).
580 44. Colinge, J., Masselot, A., Giron, M., Dessingy, T. & Magnin, J. OLAV: towards high-throughput
581 tandem mass spectrometry data identification. *Proteomics* **3**, 1454-1463 (2003).
582 45. Roy, A., Kucukural, A. & Zhang, Y. I-TASSER: a unified platform for automated protein structure
583 and function prediction. *Nat Protoc* **5**, 725-738 (2010).
584
585

Figure 1

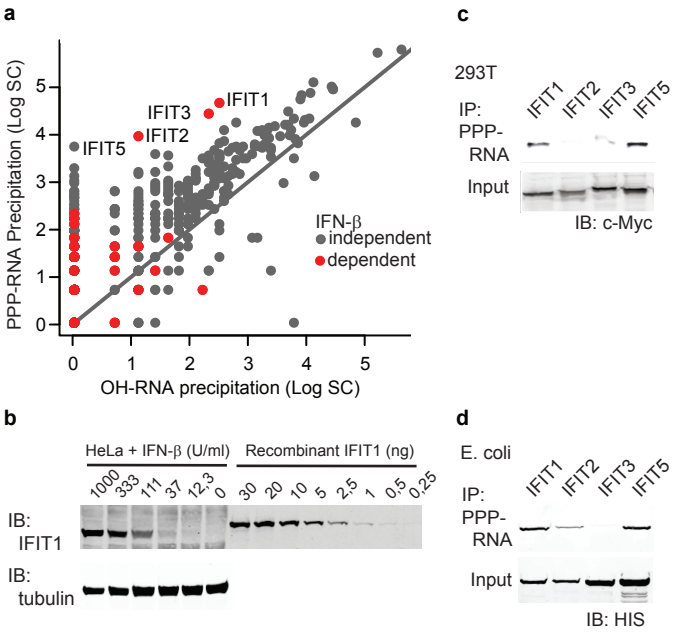
a
PPP-RNA Precipitation (Log SC)
OH-RNA precipitation (Log SC)
IFIT1
IFIT3
IFIT2
IFIT5
IFN-β
independent
dependent
b
HeLa + IFN-β (U/ml)
Recombinant IFIT1 (ng)
1000
333
111
37
12.3
0
30
20
10
5
2.5
1
0.5
0.25
IB: IFIT1
IB: tubulin
c
293T
IP:
PPP-RNA
Input
IFIT1
IFIT2
IFIT3
IFIT5
IB: c-Myc
d
E. coli
IP:
PPP-RNA
Input
IFIT1
IFIT2
IFIT3
IFIT5
IB: HIS

Figure 2

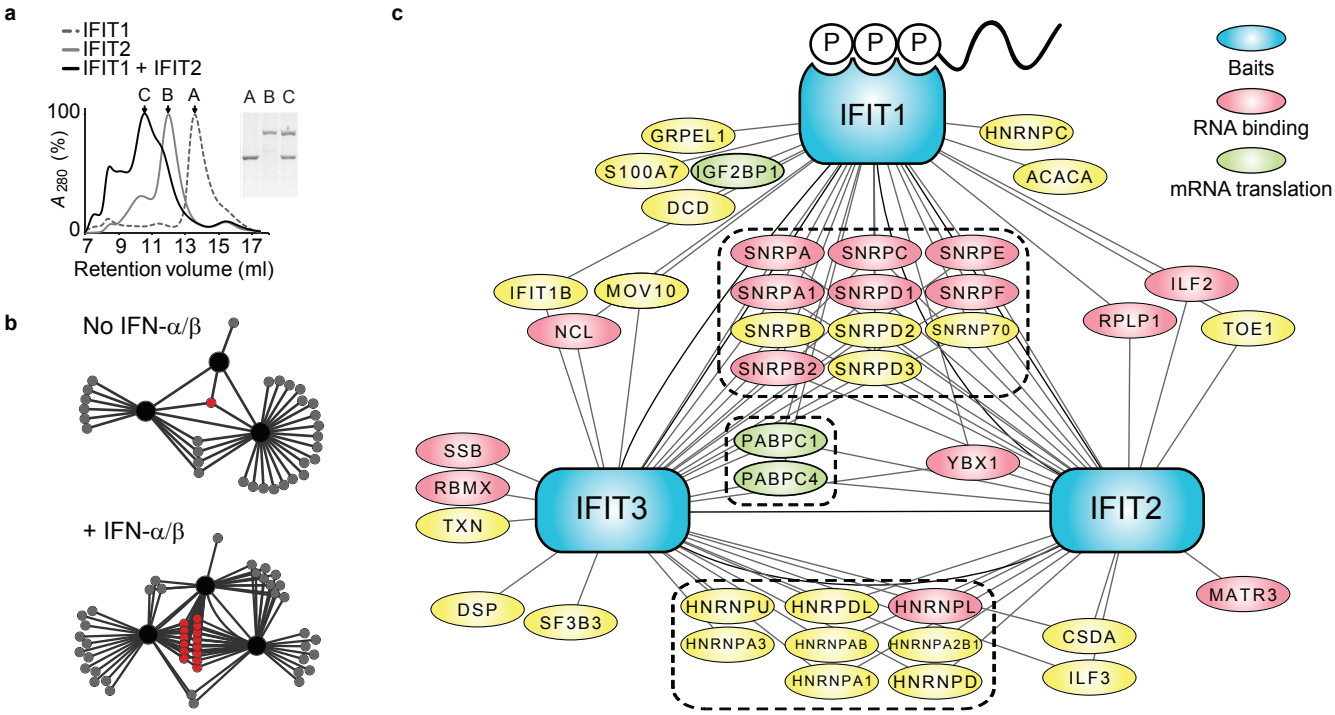
a
IFIT1
IFIT2
IFIT1 + IFIT2
C B A
A B C
100
0
A 280 (%)
7 9 11 13 15 17
Retention volume (ml)
b
No IFN-α/β
+ IFN-α/β
c
P P P
IFIT1
Baits
RNA binding
mRNA translation
GRPEL1
S100A7
IGF2BP1
DCD
HNRNPC
ACACA
SNRPA
SNRPC
SNRPE
SNRPA1
SNRPD1
SNRPF
SNRPB
SNRPD2
SNRNP70
SNRPB2
SNRPD3
IFIT1B
MOV10
NCL
ILF2
RPLP1
TOE1
PABPC1
PABPC4
YBX1
SSB
RBMX
TXN
IFIT3
IFIT2
DSP
SF3B3
HNRNPU
HNRPDL
HNRNPL
HNRNPA3
HNRNPAB
HNRNPA2B1
HNRNPA1
HNRNPD
CSDA
ILF3
MATR3

Figure 3

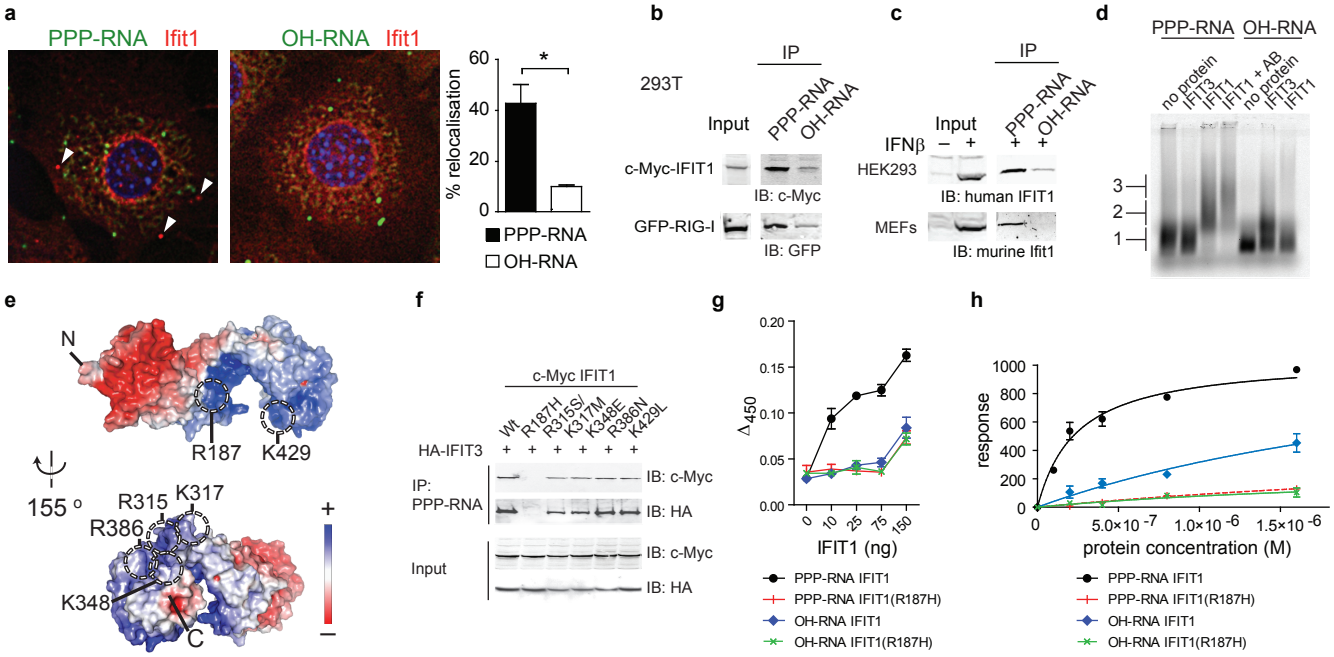
a
PPP-RNA Ifit1
OH-RNA Ifit1
% relocalisation
PPP-RNA
OH-RNA
b
293T
IP
Input
PPP-RNA
OH-RNA
c-Myc-IFIT1
IB: c-Myc
GFP-RIG-I
IB: GFP
c
IP
Input
IFNβ
HEK293
IB: human IFIT1
MEFs
IB: murine Ifit1
d
PPP-RNA OH-RNA
no protein
IFIT3
IFIT1
IFIT1 + AB
e
N
R187
K429
155 °
R315
K317
R386
K348
C
f
c-Myc IFIT1
Wt
R187H
R315S/I
K317M
K346E
R386N
K429L
HA-IFIT3
IP: PPP-RNA
IB: c-Myc
IB: HA
Input
g
Δ450
IFIT1 (ng)
PPP-RNA IFIT1
PPP-RNA IFIT1(R187H)
OH-RNA IFIT1
OH-RNA IFIT1(R187H)
h
response
protein concentration (M)
PPP-RNA IFIT1
PPP-RNA IFIT1(R187H)
OH-RNA IFIT1
OH-RNA IFIT1(R187H)

Figure 4

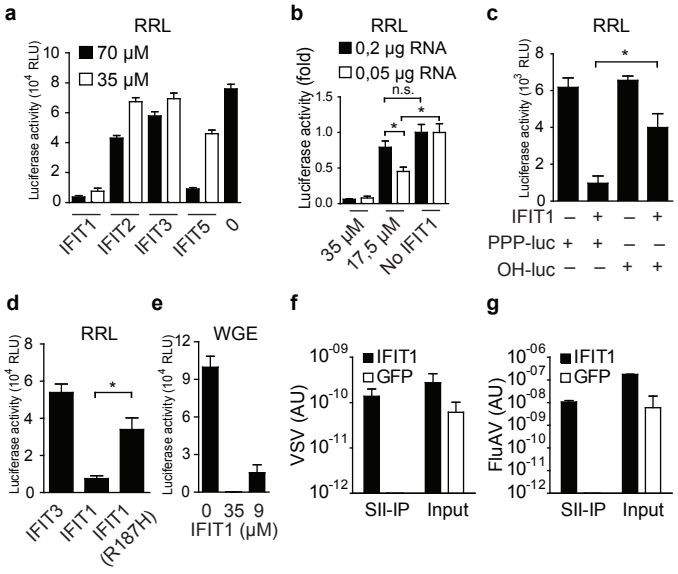
a
RRL
Luciferase activity (10^4 RLU)
70 µM
35 µM
IFIT1
IFIT2
IFIT3
IFIT5
0
b
RRL
Luciferase activity (fold)
0,2 µg RNA
0,05 µg RNA
n.s.
35 µM
17,5 µM
No IFIT1
c
RRL
Luciferase activity (10^3 RLU)
IFIT1
PPP-luc
OH-luc
d
RRL
Luciferase activity (10^4 RLU)
IFIT3
IFIT1
IFIT1 (R187H)
e
WGE
Luciferase activity (10^4 RLU)
0 35 9
IFIT1 (µM)
f
IFIT1
GFP
VSV (AU)
SII-IP
Input
g
IFIT1
GFP
FluAV (AU)
SII-IP
Input

Figure 5

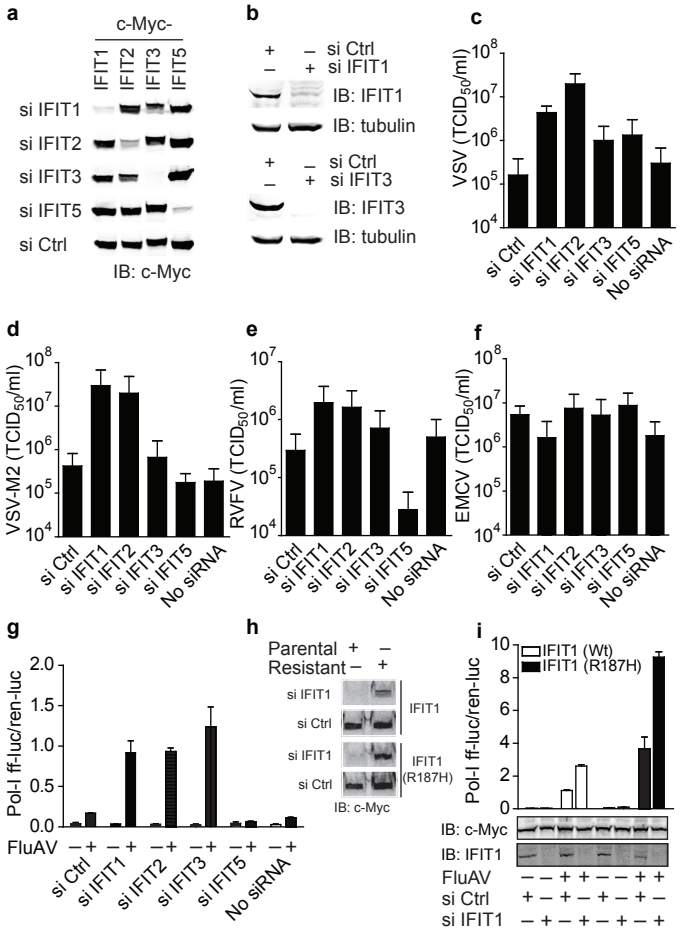
a
c-Myc-
IFIT1
IFIT2
IFIT3
IFIT5
si IFIT1
si IFIT2
si IFIT3
si IFIT5
si Ctrl
IB: c-Myc
b
si Ctrl
si IFIT1
IB: IFIT1
IB: tubulin
si Ctrl
si IFIT3
IB: IFIT3
IB: tubulin
c
VSV (TCID50/ml)
si Ctrl
si IFIT1
si IFIT2
si IFIT3
si IFIT5
No siRNA
d
VSV-M2 (TCID50/ml)
e
RVFV (TCID50/ml)
f
EMCV (TCID50/ml)
g
Pol-I ff-luc/ren-luc
FluAV
h
Parental
Resistant
IFIT1
IFIT1 (R187H)
IB: c-Myc
i
IFIT1 (Wt)
IFIT1 (R187H)
Pol-I ff-luc/ren-luc
IB: c-Myc
IB: IFIT1
FluAV
si Ctrl
si IFIT1

Figure 6

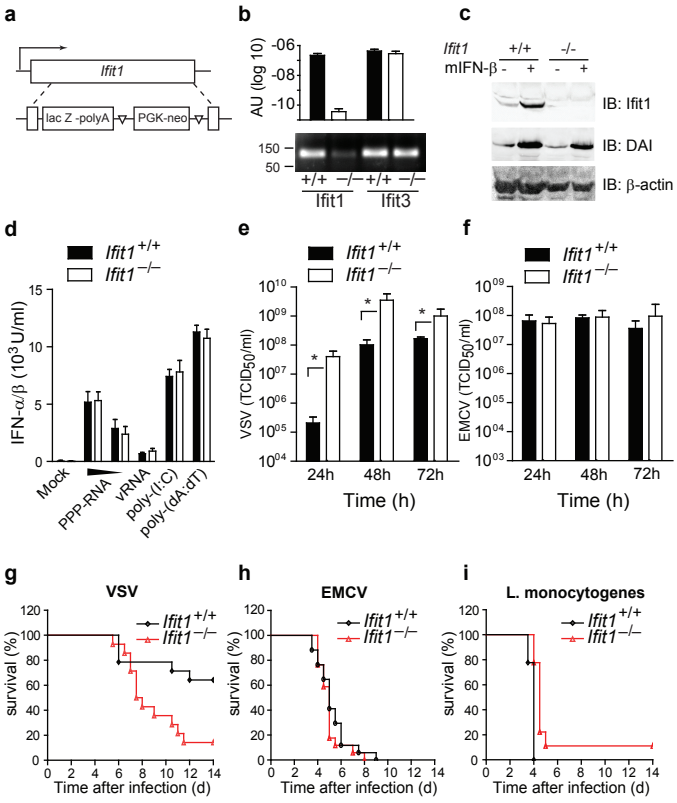
a
Ifit1
lac Z -polyA
PGK-neo
b
AU (log 10)
-06
-08
-10
150
50
+/+ −/− +/+ −/−
Ifit1
Ifit3
c
Ifit1
+/+
-/-
mIFN-β - + - +
IB: Ifit1
IB: DAI
IB: β-actin
d
Ifit1+/+
Ifit1−/−
IFN-α/β (10³ U/ml)
Mock
PPP-RNA
vRNA
poly-(I:C)
poly-(dA:dT)
e
Ifit1+/+
Ifit1−/−
VSV (TCID50/ml)
24h
48h
72h
Time (h)
f
Ifit1+/+
Ifit1−/−
EMCV (TCID50/ml)
24h
48h
72h
Time (h)
g
VSV
Ifit1+/+
Ifit1−/−
survival (%)
Time after infection (d)
h
EMCV
Ifit1+/+
Ifit1−/−
survival (%)
Time after infection (d)
i
L. monocytogenes
Ifit1+/+
Ifit1−/−
survival (%)
Time after infection (d)